https://doi.org/10.3311/PPci.23572

Periodica Polytechnica Civil Engineering, 68(2), pp. 669–683, 2024

Improving Corrosion Resistance and Prolonging the Service Life of High-performance Concrete Structures Using Fly Ash and Ground Granulated Blast-furnace Slag

Quan Van Ho[1*], Trong-Phuoc Huynh[2]

[1] Department of Civil Engineering, University of Technology and Education - The University of Danang, 48 Cao Thang, Danang 550000, Vietnam
[2] Faculty of Civil Engineering, College of Engineering, Can Tho University, Campus II, 3/2 Street, Ninh Kieu District, Can Tho City 94000, Vietnam
[*] Corresponding author, e-mail: hvquan@ute.udn.vn

Received: 03 October 2023, Accepted: 11 December 2023, Published online: 23 February 2024

Abstract

This study investigates the impact of ground granulate blast-furnace slag (GGBFS) and fly ash (FA) on both the corrosion resistance of steel reinforcement, assessed through the accelerated macrocell corrosion test (AMCT), and the durability characteristics of high-performance concrete (HPC). Additionally, the study encompasses an analysis of various concrete properties, including the pH of fresh concrete mixtures as well as water absorption, chloride permeability, and surface resistivity (SR) in hardened concrete specimens. Microstructure analysis on HPC specimens as well as the service life prediction of RCS were also performed in this study. Test results show that the HPC incorporating 35% GGBFS or 35% GGBFS + 20% FA as cement replacement resulted in a lowered pH of fresh mixtures while water absorption and chloride permeability of these specimens increased significantly. In addition, the incorporation of 35% GGBFS or 35% GGBFS + 20% FA concurrently enhanced the SR of HPC specimens. Moreover, these HPC specimens exhibited better corrosion resistance ability as their respective AMCT values were about 1.54 and 1.45 times higher than that of the control specimen. Further, the research highlighted a substantial extension in the corrosion initiation time of concrete structures employing 35% GGBFS or 35% GGBFS + 20% FA, about 3 and 6 times longer than the HPC without GGBFA and FA, respectively. The experimental results, confirmed by the substantial microstructural enhancement in the HPC containing GGBFS and FA, also demonstrated a close interplay between durability and other concrete properties such as water absorption, chloride permeability, and SR.

Keywords

high-performance concrete, ground granulated blast-furnace slag, fly ash, corrosion resistance, service life prediction

1 Introduction

The corrosion of steel reinforcement within concrete, often referred to as accelerated macrocell corrosion (AMCT), stands as a prominent contributor to the premature deterioration of reinforced concrete structures (RCS), thereby compromising their lifespan and structural integrity [1–3]. This corrosion phenomenon assumes a pivotal role in shaping the longevity and robustness of such structures [4]. The concrete cover plays a central role in governing the strength and corrosion protection of the RCS. Moreover, the internal environment of concrete characterized by a high alkaline pH range of 12–13, facilitates the formation of a passive iron oxide film (γ-FeOOH) on the surface of steel reinforcement. This passive iron oxide film serves as a protective barrier, shielding the reinforcement from direct exposure to oxygen and corrosive agents [4, 5]. AMCT incidents within concrete frequently arise from a decline in the surface alkalinity of the reinforcement, attributed to concrete carbonation or the substantial presence of chloride ions within the concrete matrix [6].

The extent of reinforcement corrosion within marine RCS is contingent upon a multitude of factors, encompassing not only concrete quality (i.e., water-to-binder ratio, binder type, and construction and curing conditions), the thickness of the concrete cover, and reinforcement type but also influenced by the composition of seawater (i.e., salinity), prevailing climatic conditions (i.e., temperature and freeze-thaw cycles), wave dynamics, wind patterns, and various exposure conditions (i.e., full flood zones, tidal zones, and splash zones) [7]. Vietnam, located in the tropical area, boasts a coastline spanning approximately

Cite this article as: Ho, Q. V., Huynh, T.-P. "Improving Corrosion Resistance and Prolonging the Service Life of High-performance Concrete Structures Using Fly Ash and Ground Granulated Blast-furnace Slag", Periodica Polytechnica Civil Engineering, 68(2), pp. 669–683, 2024. https://doi.org/10.3311/PPci.23572

3,200 kilometers from the North to the South, characterized by a marine environment typified by high temperatures, humidity, frequent rainfall, and the prevalence of storms, rendering it particularly susceptible to intensified reinforcement corrosion [8, 9]. As substantiated by previous surveys in Vietnam [9, 10], numerous RCS situated in coastal and island regions have suffered severe corrosion-related damage within a mere 10–20 years of operation. Consequently, the maintenance and safeguarding of the RCS necessitate substantial financial outlays, accounting for roughly 40–70% of the overall construction expenditure [10].

In efforts to mitigate damage and extend the lifespan of RCS in marine environments, high-performance concrete (HPC) enriched with cementitious materials (i.e., ground granulated blast-furnace slag (GGBFS), fly ash (FA), silica fume, etc.) were applied to diminish concrete permeability [2]. In addition to enhancing concrete durability, the incorporation of cementitious materials into HPC serves the dual purpose of reducing environmental impact by utilizing industrial by-products, thereby curbing the depletion of natural resources, mitigating ecological pollution, and yielding economic benefits [11, 12].

Numerous studies worldwide have investigated the incorporation of GGBFS and FA into concrete to enhance its resistance to AMCT [13–15]. So far, the inclusion of GGBFS as a partial replacement for ordinary Portland cement (PC) in concrete (mostly 25–60% by weight) has demonstrated a reduction in chloride permeability as well as chloride diffusion coefficient and an improvement in AMCT resistance [6, 16, 17]. Moreover, the utilization of GGBFS has been found to lower the pH of fresh concrete [17], and the AMCT resistance of concrete containing GGBFS was notably enhanced with extended moist curing periods [6]. Besides, previous studies affirm that FA incorporation raised pH levels, diminished chloride permeability, and augmented AMCT resistance. In detail, Boğa and Topçu [4] utilized FA to replace PC at levels of 15, 30, and 45% in concrete mixtures and found a reduction in chloride permeability and significant enhancement in AMCT resistance under extending moist curing time. They also confirmed that replacing the PC with 15% FA was optimal. Zafar and Sugiyama [18] employed FA as a substitute for 15 and 30% of PC in concrete. As a result, the reduction in chloride diffusion coefficients and the critical chloride threshold for AMCT was observed. Also, the corrosion initiation time was recorded. Prolonged moist curing of FA-infused concrete led to heightened critical chloride thresholds and significant improvements in AMCT initiation time [3]. Montemor et al. [19] used FA to partially replace PC at levels of 15, 30, and 50% and found that a 30% FA replacement level significantly boosted AMCT resistance. Hussain et al. [20] introduced 25% FA as a replacement for PC in mortar and noted the improvement in AMCT resistance during the extended curing period. Additionally, Sun et al. [21] utilized GGBFS and FA to substitute 10–30% of PC in HPC and reported the reduction in the pH of fresh concrete mixtures as the GGBFS and FA replacement ratios increased, further leading to the decreased corrosion rate and improved AMCT resistance in HPC.

Besides the positive impact of FA inclusion on the enhancement of AMCT resistance in concrete as previously mentioned, it is worth noting that some studies have proposed that FA may not consistently improve or may even reduce AMCT resistance. For instance, Saraswathy et al. [22, 23] incorporated FA as a replacement for 10–40% of PC in concrete and found that untreated FA resulted in reduced pH of fresh concrete mixtures while increasing chloride permeability and decreasing AMCT resistance of hardened concrete. On the other hand, using treated FA notably improved the chloride permeability and AMCT resistance of concrete. Ha et al. [24] also investigated AMCT resistance in concrete with FA replacing 10–50% of PC and noted the decrease in pH with higher FA content. The results of their study showed that concrete containing 10–30% FA exhibited a comparable corrosion rate and AMCT resistance to normal concrete, while the introduction of 40–50% FA led to an increased corrosion rate and a significant reduction in AMCT resistance.

While extensive research has been conducted on the AMCT resistance of normal concrete incorporating GGBFS and FA, investigations specifically focusing on HPC in this context have remained somewhat limited. Notably, in Vietnam, only a study by Huyen et al. [10] has addressed this area along with assessments of water absorption (WA) and chloride permeability but the surface resistivity (SR) of concrete was not examined. Therefore, the present study was performed to comprehensively evaluate the AMCT resistance resulting from chloride penetration in HPC enhanced with either GGBFS or a mixture of GGBFS and FA, with a specific orientation toward potential applications in marine construction. In this pursuit, the research entailed the replacement of PC with 35% GGBFS and 35% GGBFS + 20% FA. Hence, the investigation encompassed the analysis of fresh concrete mixture pH, as well as the determination and assessment of

mechanical strength, WA, chloride permeability, SR, and AMCT resistance in hardened concrete. Additionally, the service life prediction of RCS and the observation of the concrete microstructure were conducted in this study to verify the effectiveness of using GGBFS and FA in HPC.

2 Materials and experimental methods

2.1 Materials

Binder materials used for the preparation of HPC specimens consisted of grade-50 PC (specific gravity: 3.12 g/cm^3, 28-day compressive strength: 53.8 MPa, Blaine fineness: 3480 cm^2/g) in accordance with TCVN 2682:2020 [25], type-S95 GGBFS (specific gravity: 2.87 g/cm^3, 28-day strength activity index: 98%, Blaine fineness: 5145 cm^2/g) in accordance with TCVN 11586:2016 [26], and type-F FA (specific gravity: 2.12 g/cm^3, 28-day strength activity index: 87.1%, Blaine fineness: 3285 cm^2/g) in accordance with TCVN 10304:2014 [27]. The chemical compositions of these binder materials are shown in Table 1.

Fine and coarse aggregates used in this study were river sand (fineness modulus: 2.54, density: 2.65 g/cm^3, WA rate: 0.42%) and crushed stone (particle size range: 4.75-19 mm, density: 2.72 g/cm^3, WA rate: 0.22%), respectively. It is noted that all of the aggregates used for preparing HPC specimens were in saturated surface dry condition and their grain size distribution well conformed to TCVN 7570:2006 [28].

Tap water in accordance with TCVN 4506:2012 [29] was used as mixing water. Type-G superplasticizer (SP, pH: 6.94, density: 1.06 g/cm^3, solid component: 20.37%) in accordance with ASTM C494 was used to modify the workability of fresh HPC mixtures.

In this study, the mixture proportions of HPC as shown in Table 2 were designed following the guidelines of the ACI 211.4R standard [30] with a fixed SP content of 1.35% of binder weight and constant water-to-binder ratio of 0.3. In which, the control HPC (S0F0) was designed with a target compressive strength of 70 MPa at 28 days. To investigate the effectiveness of using GGBFS and FA as mentioned in Section 1, PC in the S0F0 mixture was partially replaced with 35% GGBFS (S35F0 mix) and 35% GGBFS + 20% FA (S35F20 mix). It is noted that the replacement ratios of GGBFS and FA were selected based on the optimal suggestion of the previous studies [11, 31].

Table 1 Chemical composition of PC, GGBFS, and FA

Chemical composition (wt.%)	PC	GGBFS	FA
CaO	64.1	39.2	3.8
SiO_2	20.4	35.2	54.6
Fe_2O_3	3.9	0.3	5.9
Al_2O_3	5.0	12.3	23.0
MgO	0.8	7.5	0.8
K_2O	0.7	0.7	3.3
Na_2O	0.1	0.4	0.5
SO_3	2.1	1.2	0.2
Cl^-	-	0.02	0.01
Loss on ignition	1.6	0.9	6.3
Others	1.3	2.3	1.6

Table 2 Mixture proportions of HPC

Ingredients (kg/m^3)	S0F0	S35F0	S35F20
PC	500	325	225
GGBFS	0	175	175
FA	0	0	100
Sand	710	697	662
Stone	1120	1120	1120
Water	150	150	150
SP	6.75	6.75	6.75
Slump (cm)	8	12	15
f'_c (MPa)	74.5	76.3	71.4

f'_c: Compressive strength at 28 days

2.2 Experimental methods

2.2.1 Preparation of test specimens

Cylindrical concrete specimens with diameters of 100 and 150 mm and heights of 200 and 300 mm were prepared and moist-cured following TCVN 3105:2022 [32] until the day of testing. The concrete specimens with a diameter of 150 mm and height of 300 mm were used for testing concrete compressive strength while the specimens with a diameter of 100 mm and height of 200 mm were used for splitting tensile strength, WA, chloride permeability, and SR tests.

To evaluate the corrosion resistance of steel reinforcement, cylindrical molds with a diameter of 100 mm and height of 200 mm were used to prepare the test specimens. A steel bar of 10 mm diameter and 250 mm long was placed in the center and positioned 50 mm from the bottom of each mold (see Fig. 1 (a)). After that, fresh concrete was poured into ½ mold and placed the mold on a vibration table for compaction. Repeating the same steps for the rest of ½ mold. Importantly, the steel bar should remain in the center and vertical within the mold during vibration. After 24 h, the test specimens (see Fig. 1 (b)) were removed from the mold and then cured in water for 14 days and subsequently left to dry in a laboratory environment at 25±2 °C for the next 14 days.

(a)

(b)

Fig. 1 (a) Cylindrical molds and (b) concrete specimens prepared for testing corrosion resistance of steel reinforcement

2.2.2 The pH measurement

The pH of the fresh concrete mixture was measured using a handheld HANNA HI98194 device (see Fig. 2), which features a readout display with a pH scale ranging from 0 to 14, and boasts an accuracy level of ±0.002 pH. For the pH measurement, the device's measuring probe was first inserted into the center of the mold with a diameter of 100 mm and height of 200 mm (see Fig. 2), and then the fresh concrete was subsequently poured into the mold, ensuring that the probe was completely covered by the fresh concrete with the use of a vibration table. Finally, the pH value was recorded after approximately 35–40 minutes when the value displayed on the device was stable.

2.2.3 Compressive and splitting tensile strengths

The tests of compressive and splitting tensile strengths were performed at 28 and 56 days following the TCVN 3118:2022 [33] and ASTM C496-96 [34], respectively. It's important to note that the reported value for each concrete type represents the average value derived from testing three concrete specimens at each testing age.

Fig. 2 The pH measurement of fresh concrete mixtures

2.2.4 Water absorption

The WA of the concrete was measured at 28 and 56 days of specimen age in accordance with ASTM C642-21 [35]. For this test, cylindrical specimens measuring 100 mm in diameter and 50 mm in thickness that were extracted from the specimens with a diameter of 100 mm and height of 200 mm were used. The WA rate of each type of concrete was calculated using the following formula:

$$\mathrm{WA}(\%) = \frac{B - A}{A} \times 100, \tag{1}$$

where A is the mass of the specimen after drying (g) and B is the mass of the saturated specimen after 24 h immersed in boiling water (g). The reported WA rate for each concrete mixture was the average value of three tested specimens.

2.2.5 Surface resistivity and chloride permeability

Chloride permeability assessment for the HPC was conducted at 28 and 56 days using cylindrical specimens following the ASTM C1202-19 standard [36]. Prior to testing, the concrete specimens were subjected to waterproofing and vacuum treatment procedures as per the standard guidelines. Besides, the test of SR was also performed at 28 and 56 days using cylindrical specimens with a diameter of 100 mm and height of 200 mm in accordance with the AASHTO T95 standard [37]. The reported values for both SR and chloride permeability represent the average value obtained from three tested specimens.

2.2.6 Corrosion resistance of steel reinforcement

The determination of AMCT was carried out in accordance with the NT Build 356 report [38]. The prepared specimens (see Fig. 1 (b)) were immersed in a tank with a 3% NaCl solution, noting that the solution level in the tank was maintained 30 mm below the top of the test specimens during the experiment. To ensure equal voltage across the test specimens, they were parallelly connected. An electrical current passed through the test specimens through 10 Ω resistors, with a consistent applied voltage of 10 V. Current measurements, accurate to 0.1 μA, were recorded using an ammeter connected to the resistors' terminals (see Fig. 3 (a)). The current intensity was recorded initially and every 12 hours until the concrete specimens eventually cracked due to corrosion. Six specimens of each concrete mixture were subjected to the AMCT test. To account for evaporation, the NaCl solution in the tanks was periodically replenished to maintain the prescribed level, and the solution was replaced every two weeks during the initial 28 days to prevent pH changes resulting from alkalinization. Following the 28-day mark, the pH of the solution stabilized, prompting monthly solution renewals.

(a)

(b)

Fig. 3 (a) Test setup of corrosion resistance of steel reinforcement and (b) test specimens after the experiment

The duration from the initiation of chloride ion penetration, leading to corrosion in the test specimens, until the first appearance of cracks is referred to as the AMCT time, also known as deterioration occurrence time. This time interval is determined by analyzing a chart depicting current intensity over time, in conjunction with visual observations of cracks emerging on the concrete specimens. It is calculated from the inception of the experiment until the point when cracks start to manifest (signifying a sudden increase in current). The anti-AMCT durability of the S35F0 and S35F20 specimens, in comparison to the control S0F0 specimen, was assessed using the following formula:

$$Q_i = \frac{t_{ami}}{t_{am\text{S0F0}}}, \tag{2}$$

where t_{ami} (days) is the average deterioration occurrence times for the S35F0 and S35F20 specimens and $t_{am\text{S0F0}}$ (days) is the deterioration occurrence times of the S0F0 specimen, averaged for 6 samples.

2.2.7 Service life prediction

According to TCVN 12041:2017 [39], the design equation used to predict the service life of RCS without considering maintenance (time to the onset of steel reinforcement corrosion) is as follows:

$$\left(C_S - C_0\right)\left(1 - erf\left(\frac{x}{\sqrt{4 \times D_a(t) \times t}}\right)\right) + C_0 = C_{Cr} \tag{3}$$

$$D_a(t) = D_{a28}\left(\frac{t_{28}}{t}\right)^m, \tag{4}$$

where: x represents the thickness of the concrete cover (mm), with $x_{\min} \geq 50$ mm [7]; C_0 denotes the initial chloride content at the surface of reinforcement in concrete, including raw materials, measured as a percentage of the concrete volume, and in this case, $C_0 = 0$; *erf* stands for the error function; t signifies the time taken for the onset of corrosion of the reinforcement (year); D_{a28} is the apparent chloride diffusion coefficient of concrete at 28 days (mm^2/year); $D_a(t)$ represents the apparent chloride diffusion coefficient of concrete at time t (mm^2/year). As per Life-365 [40], $D_a(t)$ reaches its minimum value when $t = 25$ years, and for $t > 25$ years, it remains constant;

C_{Cr} denotes the chloride concentration that leads to corrosion of the reinforcement (% by weight of concrete); C_S represents the chloride concentration at the concrete surface (% by volume of concrete); m is the chloride diffusion attenuation factor over time.

The critical chloride concentration causing corrosion of steel reinforcement (C_{Cr}) was taken based on the TCVN 12041:2017 [39]. Thus, the C_{Cr}^{S0F0} = 0.45% binder weight (0.091% concrete weight); C_{Cr}^{S35F0} = 0.30% binder weight (0.061% concrete weight); and C_{Cr}^{S35F20} = 0.20% binder weight (0.041% concrete weight).

According to ACI Committee 365 [40], the coefficient m for S0F0 concrete, m^{S0F0} = 0.20; for S35F0 concrete, m^{S35F0} = 0.40; and for S35F20 concrete, m^{S35F20} = 0.56. A similar coefficient value was also suggested by previous studies [41, 42].

Considering a part of the RCS exposed in the tidal area close to the water's edge, the surface chloride concentration (C_S) of the RCS as a function of time is shown in Table 3.

The surface chloride concentration C_S can be expressed according to the exponential law [43, 44], from the data in Table 3, a regression equation with R^2 = 0.998 is obtained as follows:

$$C_S(t) = 0.127 \times t^{0.2376}. \quad (5)$$

The apparent chloride diffusion coefficient D_{28} of concrete can be approximately calculated according to the empirical formulas of Berke and Hicks [45] from the chloride permeability at 28 days Q_{28} as follows:

$$D_{28} = 1.03 \times 10^{-14} \left(Q_{28}\right)^{0.84} \ \left(\mathrm{m^2/s}\right). \quad (6)$$

Combining Eqs. (3)–(6) to calculate the time to start corrosion of steel reinforcement of the RCS (t_{corr}).

2.2.8 SEM analysis

SEM analysis was conducted to examine the microstructure of the concrete specimens. After 28 days, small samples of about 5 mm were extracted from the concrete specimens. These samples were carefully prepared by cutting, polishing, and coating with a thin layer of conductive material (i.e., platinum) to prevent charging during imaging [11]. SEM images were acquired using a high-resolution SEM operating at an acceleration voltage of 10 kV at 3000× magnification.

Table 3 Chloride concentration at the surface of RCS in tidal areas [39]

Exposure time (years)	10	20	30	40	50
C_S (% of concrete volume)	0.299	0.398	0.453	0.506	0.551

3 Results and discussion

3.1 The pH of fresh concrete mixtures

The pH values of the fresh concrete mixtures are illustrated in Fig. 4. Notably, the pH values of the S35F0 and S35F20 mixtures decreased significantly, with reductions of 2.09% and 5.11%, respectively, compared to the S0F0 mixture. This drop in pH can be attributed to the replacement of cement with 35% GGBFS, resulting in a decrease in the volume of PC within the mixtures. Additionally, GGBFS contains a lower CaO content (39.2%) compared to PC (64.1%), which contributes to reduced alkalinity in the mixtures and consequently a lower pH. Interestingly, the pH decrease intensified when 55% PC was replaced with 35% GGBFS and 20% FA. This is because the PC content continued to decrease, and FA has a very low CaO content (3.8%) relative to PC. Furthermore, the pH reduction may also result from GGBFS and FA absorbing some $Ca(OH)_2$ through the pozzolan reaction [3], aligning with findings from prior studies [16, 21, 22].

Although mixtures containing GGBFS and FA exhibited lower pH levels, they still maintained a pH value of above 12, which is higher than the critical pH threshold for breaking the passive film on embedded reinforcement surfaces (ranging from 11.5 to 12.0) [4]. This suggests that the pH decrease does not significantly hinder the formation of the passive oxide film on the reinforcement surface within the concrete samples. However, the decrease

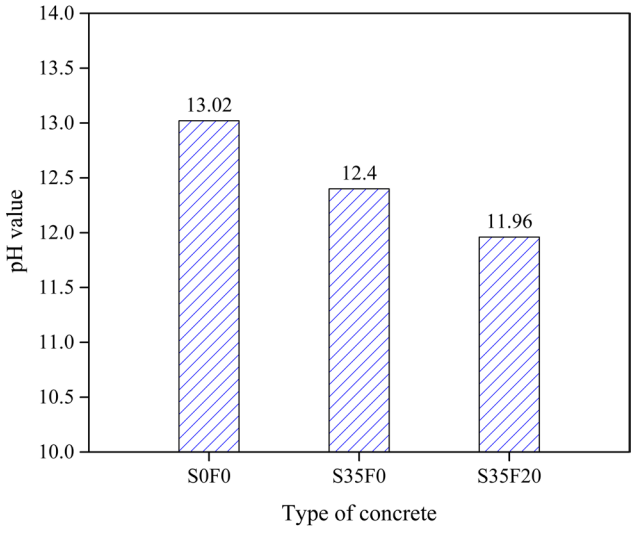

Fig. 4 The pH of fresh concrete mixtures

in pH implies a reduction in the amount of $Ca(OH)_2$ in the concrete, potentially leading to a decrease in the critical chloride threshold that triggers AMCT [3, 18], which could pose challenges for the S35F20 samples.

3.2 Water absorption

The WA of both S35F0 and S35F20 concretes (Fig. 5) exhibited a significant reduction compared to the S0F0 concrete. At 28 days, the WA of the S35F0 and S35F20 specimens decreased by 14.05% and 16.39%, respectively, while the 56-day values were 14.79% and 20.9% when compared to the S0F0 concrete. This notable decrease in WA in the S35F0 and S35F20 specimens was attributable to the micro aggregates filling the pores between particles and the pozzolanic reaction of GGBFS and FA with the $Ca(OH)_2$ hydration products from the cement, resulting in the formation of additional calcium-silicate-hydrate (C-S-H) gels. Thus, reduced porosity of the system, stemming from these effects, leads to lower WA [1, 11, 46]. Moreover, it's worth noting that the S35F20 concrete exhibited a slightly lower WA level at 28 days (approximately 2.72%) compared to the S35F0 concrete. However, this difference becomes more pronounced at 56 days, with a reduction of 7.3%, suggesting that the addition of FA has a particularly beneficial impact on the later stages of concrete performance.

3.3 Compressive and splitting tensile strength

The compressive and splitting tensile strengths of the concrete specimens at 28 and 56 days are shown in Fig. 6. The results depicted in Fig. 6 (a) reveal that the compressive strength of the S35F0 concrete consistently ranked as the highest, followed by the S0F0, and then the S35F20

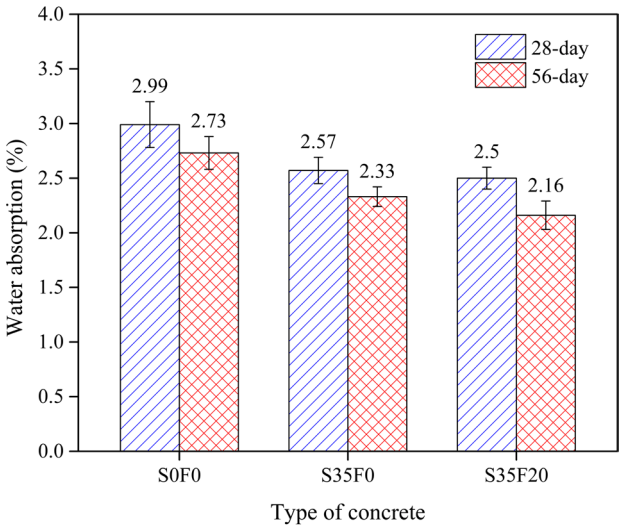

Fig. 5 WA of concrete specimens

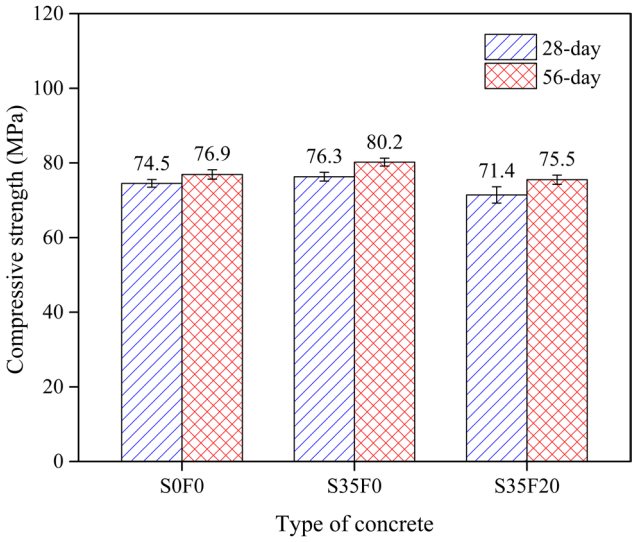

(a)

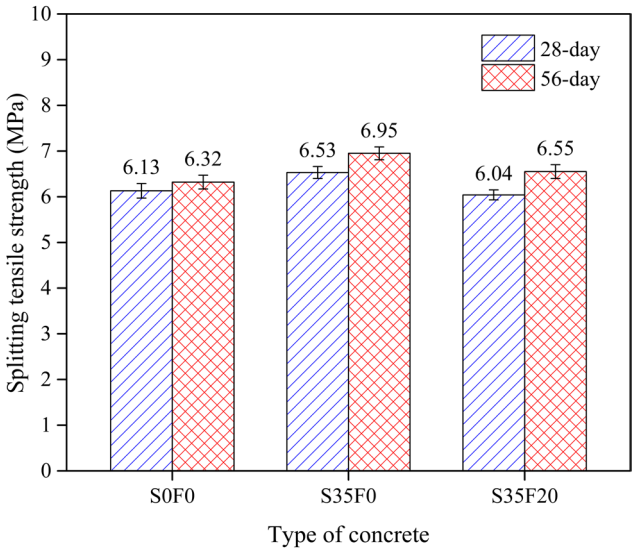

(b)

Fig. 6 (a) Compressive strength and (b) splitting tensile strength of concrete specimens

concrete. Specifically, at both 28 and 56 days, the S35F0 concrete displayed compressive strengths that were 2.43% and 4.39% higher, respectively, than those of the S0F0 concrete. Conversely, the S35F20 concrete exhibited compressive strengths that were 4.19% lower at 28 days and 1.81% lower at 56 days compared to the S0F0 concrete. Besides, the experimental results also found that the use of 35% GGBFS alone to replace PC proved more effective than combining 35% GGBFS with 20% FA. This discrepancy can be attributed to GGBFS's amphoteric nature, possessing both hydraulic and pozzolanic properties, resulting in self-hydration and the creation of C-S-H gels similar to PC but at a slower rate. Conversely, the addition of 20% FA

slowed down the strength development due to its slower reaction kinetics. Type-F FA is purely pozzolanic and almost cannot self-hydrate to form C-S-H as GGBFS does. Consequently, higher FA content resulted in a slower rate of mechanical strength development. However, at 56 days, the compressive strength of the S35F20 concrete was comparable to the S0F0's strength, indicating the advantage of FA addition in the long-term run of concrete.

In Fig. 6 (b), the S35F0 concrete also exhibited the highest splitting tensile strength, with values at 28 and 56 days being 6.53% and 9.97% higher, respectively, than those of the S0F0 concrete. For the S35F20 concrete, the splitting tensile strength was about 1.47% lower at 28 days but 3.64% higher at 56 days compared to the S0F0 specimen. Notably, the enhancement in splitting tensile strength of concrete containing GGBFS and FA surpassed that in compressive strength. This improvement can be attributed to GGBFS and FA enhancing cohesion and reducing the occurrence of microcracks at the aggregate-cement paste interface, leading to decreased brittleness in concrete and consequently increasing its splitting tensile strength. These findings align closely with previous research [47].

3.4 Surface resistivity and chloride permeability

The SR and chloride permeability of concrete at 28 and 56 days are presented in Figs. 7 and 8, respectively. Fig. 7 illustrates that the SR levels of the S35F0 and S35F20 specimens increased significantly, with a 74.58% and 69.55% increase at 28 days and a 96.0% and 117% increase at 56 days as compared to the S0F0 specimen. Whereas, a significant reduction in chloride permeability for both S35F0 and S35F20 specimens was observed in Fig. 8 as

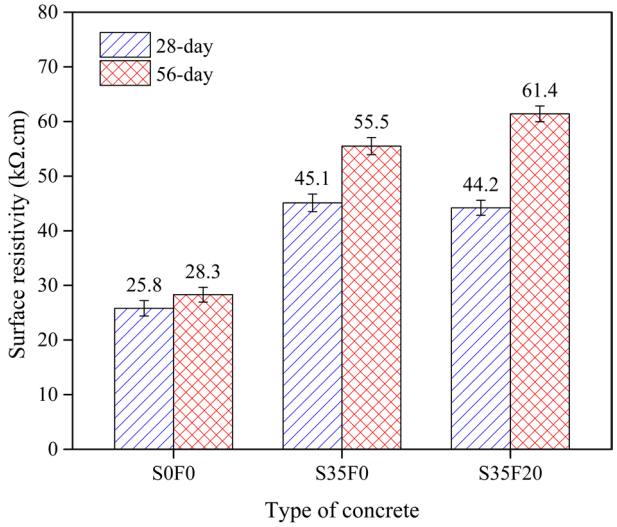

Fig. 7 SR of concrete specimens

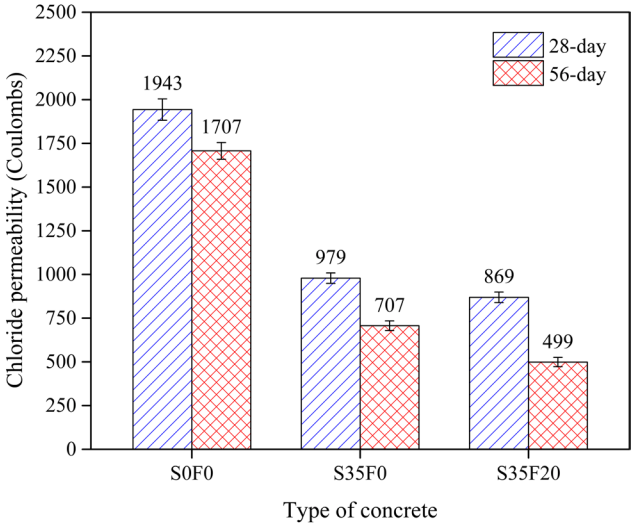

Fig. 8 Chloride permeability of concrete specimens

compared to the S0F0 concrete. For instance, at 28 days, the chloride permeability of S35F0 and S35F20 concretes decreased by 49.61% and 55.29%, respectively. At 56 days, these reductions increased to 58.59% and 70.76%, respectively, compared to the control S0F0. The notable improvements in both chloride permeability and SR in S35F0 and S35F20 specimens are primarily attributed to the reduced porosity resulting from the clinker effect and the pozzolanic reaction of GGBFS and FA with $Ca(OH)_2$, as previously explained. Additionally, the high Al_2O_3 content in GGBFS (12.3%) and FA (23.0%) promoted their ability to bind chloride more effectively than cement alone, forming Friedel salt ($3CaO{\cdot}Al_2O_3{\cdot}CaCl_2{\cdot}10H_2O$) and further contributing to reduced chloride permeability. This outcome aligns with previous research findings [11, 46, 48]. Moreover, the SEM images confirm the denser structure of the hardened concrete due to the pozzolanic reaction, supporting the results of mechanical strength, WA, SR, and chloride permeability (lately discussed in Section 3.7).

The relationships among chloride permeability, WA, and SR of concrete are depicted in Figs. 9–11. Generally, these relationships exhibited a strong linear correlation with coefficients of determination (R^2) of above 0.902. Specifically, the relationship between chloride permeability and WA is directly proportional, indicating that as one increased, the other also increased. In contrast, the relationship between chloride permeability and SR, as well as between SR and WA, is inversely proportional, signifying that as one parameter increased, the other decreased. In other words, higher WA is associated with higher chloride permeability and lower SR while lower SR is also associated with lower chloride permeability in concrete.

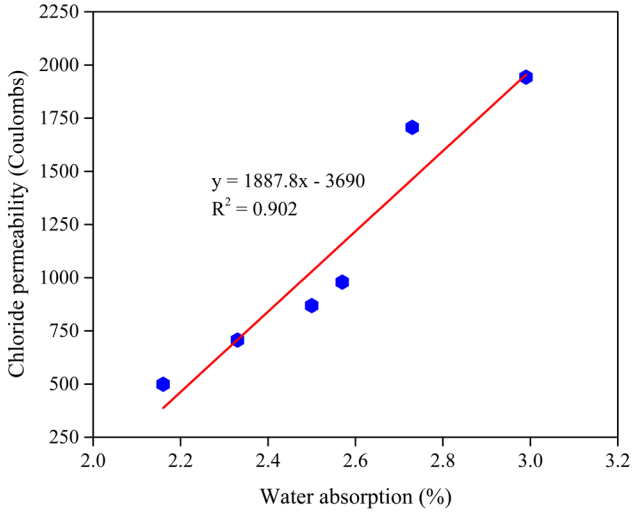

Fig. 9 Relationship between chloride permeability and WA of concrete

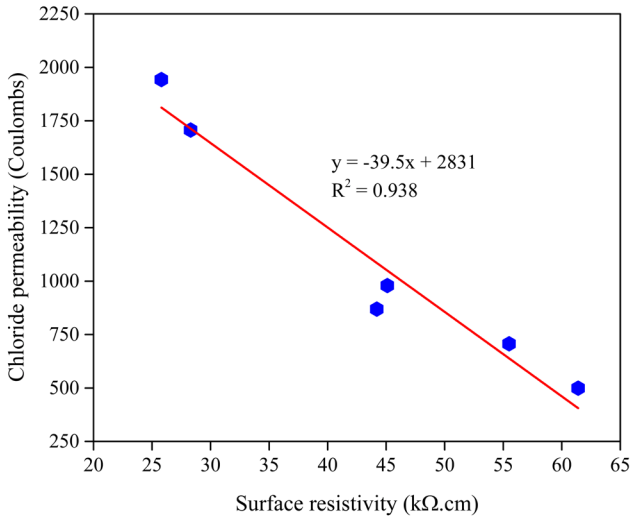

Fig. 10 Relationship between chloride permeability and SR of concrete

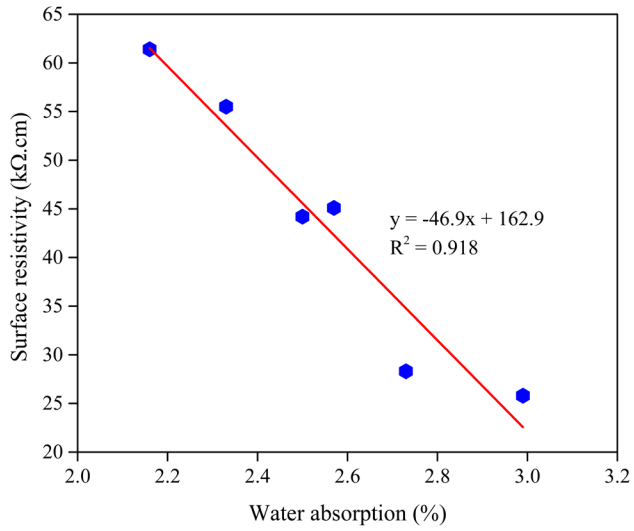

Fig. 11 Relationship between SR and WA of concrete

3.5 Corrosion resistance of steel reinforcement

The corrosion current through the concrete specimens over time is shown in Fig. 12 while Fig. 13 shows the deterioration occurrence time and durability of concrete. It could be observed that the reinforced concrete specimens using S0F0 (Fig. 12 (a)) exhibited the highest average corrosion current values, ranging from 7.0 mA to 8.0 mA, and had the shortest average deterioration occurrence times, approximately 60.33 days (see Fig. 13). In contrast, for the reinforced concrete specimens using S35F0 (Fig. 12 (b)) and S35F20 (Fig. 12 (c)), the current passing through the specimens decreased, and the deterioration occurrence times were significantly extended compared to the S0F0 specimen (see Fig. 12 (d)). In detail, the average corrosion current values for the S35F0 and S35F20 specimens were approximately 4.0–4.5 mA and 3.5–4.0 mA, respectively, with average deterioration occurrence times of about 92.92 and 87.58 days (see Fig. 13). As shown in Fig. 13, the durability of the S35F0 and S35F20 reinforced concrete specimens was found to be 1.54 and 1.45 times greater, respectively, than that of the S0F0 specimen. The improved durability of the S35F0 and S35F20 specimens was primarily attributable to their low porosity, reduced chloride permeability, and enhanced chloride binding capacity, as above explanations. However, despite the S35F20 specimen having lower WA and chloride permeability than the S35F0 specimen (see Figs. 5 and 8), the deterioration occurrence times of the S35F20 were approximately 5.34 days shorter than the S35F0 (representing a 5.74% reduction). As aforementioned, this reduction in the resistance to AMCT of the S35F20 concrete may be due to its decreased pH, resulting in a lowered critical chloride threshold, which consequently decreased the AMCT resistance of concrete.

Moreover, it's worth noting that the WA, chloride permeability, and SR tests were conducted on the samples fully cured in water for 28 days, whereas the AMCT resistance test was performed on the reinforced concrete samples cured in water for only 14 days and subsequently allowed to air dry for the next 14 days. These relatively inadequate moist curing conditions may limit the pozzolan reaction mechanism of FA in comparison with PC and GGBFS. In this case, the pozzolan reaction mainly depends on the CaO content in the system, with FA having a CaO content of 3.8%, while PC and GGBFS have CaO contents of 64.1% and 39.2%, respectively (see Table 1).

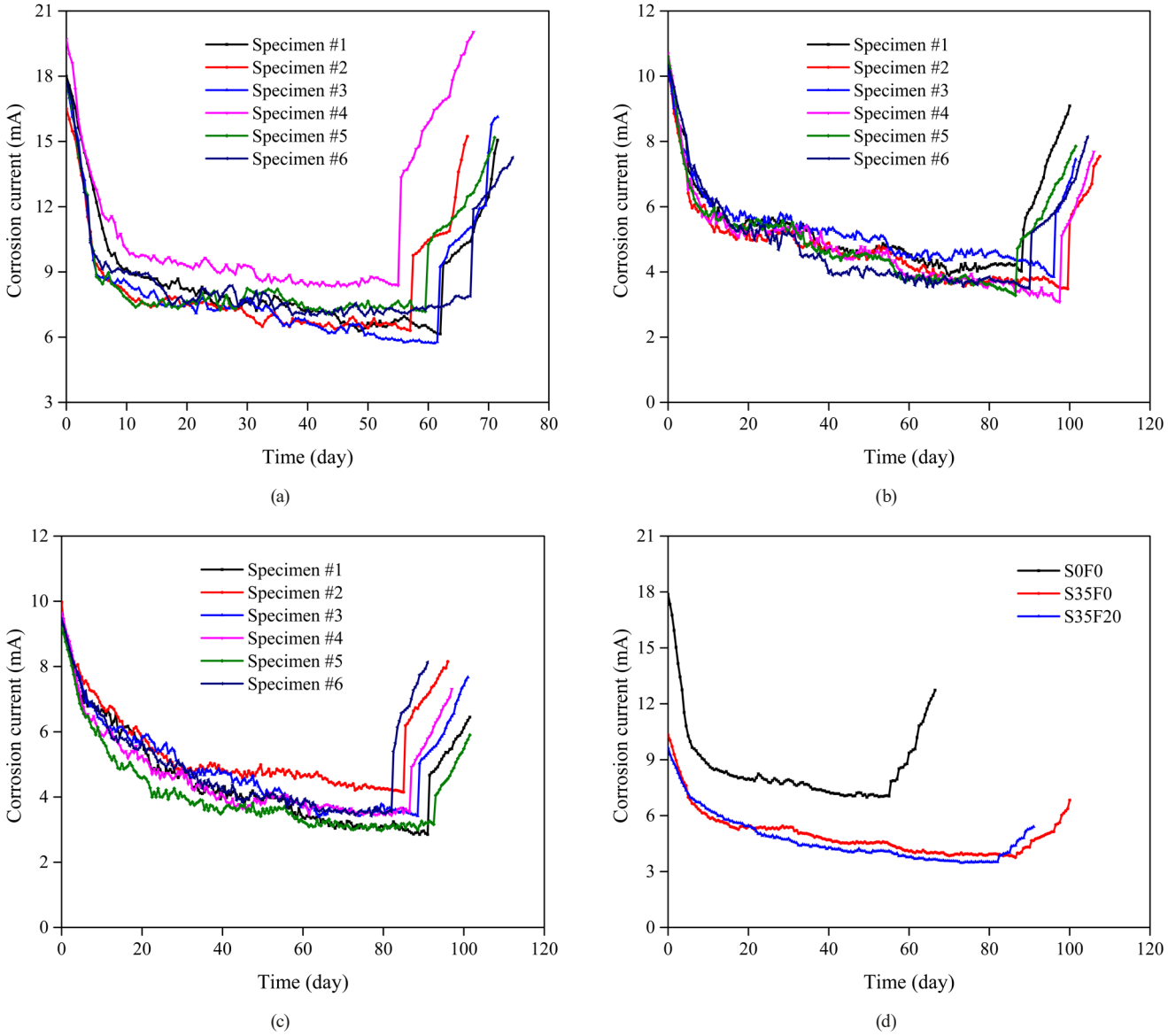

Fig. 12 Corrosion current through concrete specimens over time: (a) S0F0, (b) S35F0, (c) S35F20, and (d) comparison of three concrete types

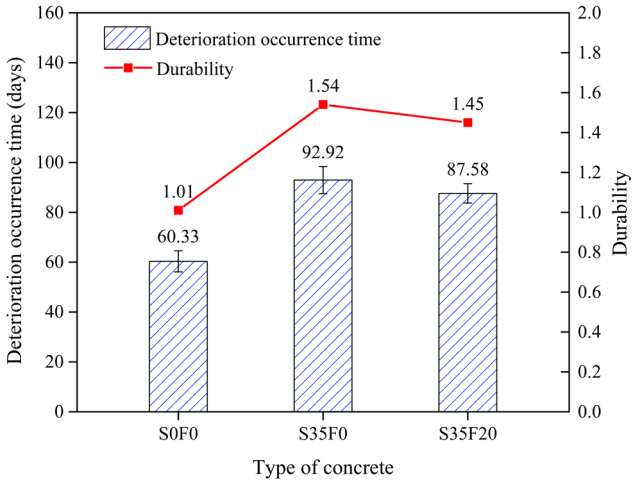

Fig. 13 Deterioration occurrence time and durability of concrete

This limitation could also contribute to the decreased AMCT resistance of concrete containing FA (S35F20) when compared to concrete containing only GGBFS (S35F0). These findings were in good agreement with the results of previous studies [22–24]. Based on the experimental results, it is suggested that the moist curing time for concrete containing FA is required to extend at least 28 days in other to enable its waterproofing ability and AMCT resistance [3, 18, 20].

Under close observation of the test results on WA (Fig. 5), SR (Fig. 7), chloride permeability (Fig. 8), and deterioration occurrence times (Fig. 13) of the three concrete types, it could be recognized that these concrete properties had good correlations. These findings illustrate

that deterioration occurrence times are inversely proportional to chloride permeability and WA degree, while they are directly proportional to the SR of concrete.

3.6 Service life prediction of RCS

In this study, the service life of RCS, indicated by the time to start the corrosion of reinforcement (denoted as t_{corr}) in the structure, is estimated in Fig. 14. As a result, the t_{corr} in the RCS using S35F0 and S35F20 mixtures was significantly prolonged as compared to that of the RCS using the S0F0 mix. On the other hand, it could be observed that when the thickness of the protective concrete layer (x) for S0F0 reached its maximum value (x_{max} = 80 mm), the t_{corr} was only 32.2 years. However, the t_{corr} was recorded at 55.5 years and 109.9 years for the S35F0 and S35F20 structures with x = 55 mm only. When increasing the concrete cover to the maximum allowable thickness of 80 mm, the t_{corr} was significantly extended to 102.8 and 209.4 years respectively for the S35F0 and S35F20 structures.

Interestingly, despite the S0F0 concrete having a coefficient D_{a28} approximately 1.78 and 1.97 times larger than that of S35F0 and S35F20 concrete, respectively (see Section 2.2.7), its t_{corr} was much shorter because the coefficient m for the S35F0 and S35F20 was approximately 2.0 times and 2.8 times larger than that of S0F0 (see Section 2.2.7). It was also found that the t_{corr} of the S35F20 structure was about 2.0 times longer than that of the S35F0 structure due to its higher coefficient m (approximately 1.4 times larger). In practical terms, this means that RCS using the S35F0 and S35F20 mixtures is well-suited for marine structures with a service life exceeding 100 years,

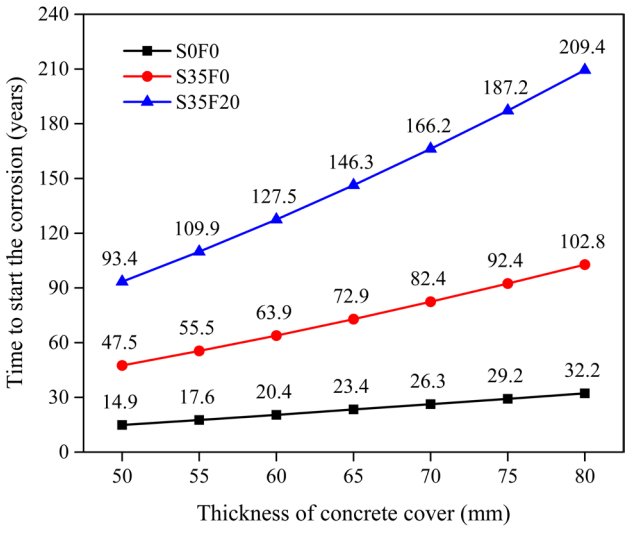

Fig. 14 Time to start corrosion of steel reinforcement in RCS

meeting the minimum design service life requirement of 50 years for coastal area-protected structures as per TCVN 12041:2017 standard [39].

3.7 SEM analysis

Fig. 15 displays the SEM images of concrete specimens at 28 days, revealing distinct microstructural characteristics for the control specimen (S0F0), 35% GGBFS replacement (S35F0), and the combination of 35% GGBFS and 20% FA (S35F20) specimens. Fig. 15 (a) reveals a traditional microstructure characteristic of HPC. The cementitious matrix appeared densely packed with well-defined hydration products, showcasing C-S-H gels. Notably, minimal porosity was observed, indicating a relatively low permeability of this concrete mix. The absence of cementitious materials like GGBFS and FA in this mix contributes to its traditional microstructural characteristics, which serve as the baseline for comparison.

On the other hand, the SEM image of the S35F0 specimen (Fig. 15 (b)) reveals distinct microstructural enhancements. The presence of GGBFS fostered the formation of additional C-S-H gels within the cementitious matrix. This phenomenon contributes to a more compact and dense microstructure with fewer voids and a refined particle packing structure, indicating improved interparticle cohesion. In other words, the inclusion of GGBFS in the mix provided a positive effect on the reduction of porosity and enhanced bonding within the concrete, making it less susceptible to chloride permeability.

Similarly, the SEM image of the S35F20 specimen (Fig. 15 (c)) also demonstrated microstructural improvements attributed to the synergistic combination of GGBFS and FA, suggesting an enhanced pozzolanic reaction. This combination resulted in a refined cementitious matrix with fewer voids and more homogeneously distributed hydration products. Interfacial interactions between the cementitious materials and the cementitious matrix were evident, further improving overall microstructural integrity. The addition of FA played a significant role in achieving a highly compacted microstructure with a substantial reduction in porosity. These microstructural enhancements were indicative of improved durability and resistance to AMCT and corrosion, particularly in marine environments.

In summary, the SEM analysis results emphasized the beneficial microstructural changes induced by the incorporation of cementitious materials (i.e., GGBFS and FA) in HPC. These changes include reduced porosity, enhanced

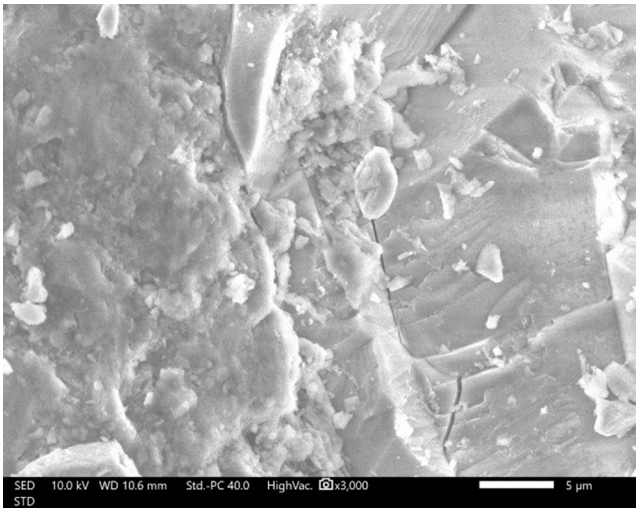

(a)

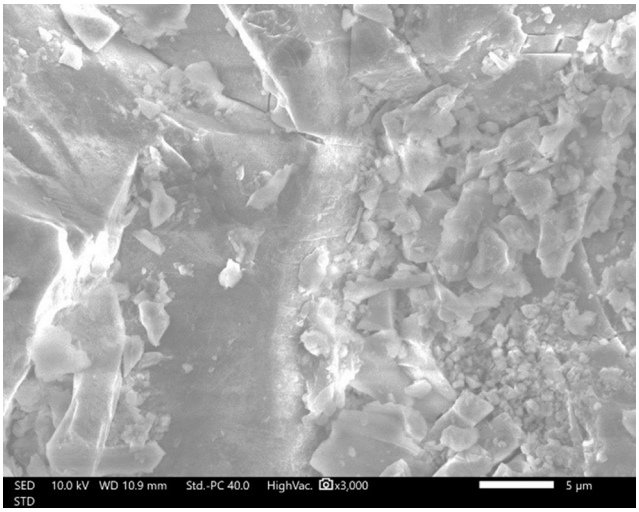

(b)

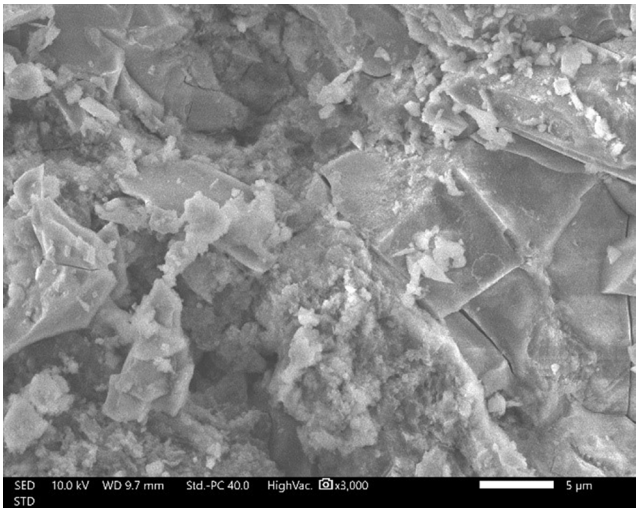

(c)

Fig. 15 SEM images of concrete at 28 days: (a) S0F0, (b) S35F0, and (c) S35F20

particle packing, and increased interparticle bonding. This study found that the combination of 35% GGBFS and 20% FA (S35F20) stands out as having the most significant impact on microstructural refinement, aligning with the study's objectives and findings regarding improved durability and corrosion resistance in marine environments.

4 Conclusions

Based on the experimental findings, the following conclusions can be drawn:

- The use of 35% GGBFS and 35% GGBFS + 20% FA to partially replace PC in HPC resulted in a reduction in the pH value of fresh concrete mixtures. However, the pH of these mixtures remains above 12.0, which did not significantly affect the formation of a passive oxide film on the surface of embedded reinforcement in concrete. Nevertheless, a pH drop below 12.0–12.5 range can lower the critical chloride threshold that causes AMCT, potentially decreasing the AMCT resistance of concrete.
- The incorporation of GGBFS and FA in HPC resulted in a significant reduction in WA and chloride permeability, along with an increase in the SR of concrete. Specifically, the WA and chloride permeability at 28 days decreased by 14.05% and 16.39% for the S35F0 specimen, and by 49.61% and 55.29% for the S35F20 specimens while the SER of these specimens increased by 74.58% and 69.55%, respectively, as compared to the control S0F0 specimen.
- The resistance to AMCT of the S35F0 and S35F20 specimens was approximately 1.54 and 1.45 times higher than that of the S0F0. As a result, it's worth noting that the durability of concrete against AMCT depended not only on WA, chloride permeability, and SR of the hardened concrete but also on the pH of the fresh concrete mixtures. Based on the experimental findings, to enhance the AMCT resistance of the concrete containing high cementitious content (i.e., 35% GGBFS and 20% FA), it is recommended to extend the moist curing period to at least 28 days.
- The t_{corr} for RCS using S35F0 and S35F20 concrete was significantly longer, about 3.0 times and 6.0 times greater, respectively, as compared to the S0F0 concrete. Moreover, the t_{corr} of structures using the S35F20 mixture was approximately 2.0 times longer than that of S35F0 concrete. These findings suggested that both S35F0 and S35F20 mixtures

were not only good applications for normal construction works but also suitable choices for marine construction projects.

- SEM analysis revealed substantial microstructural enhancements in the concrete mixtures incorporating cementitious materials as a PC substitution. SEM observations demonstrated that HPC specimens with GGBFS and FA exhibited a reduction in porosity, an enhancement in interparticle cohesion, and refined particle packing structures. These microstructural changes align with the study's emphasis on enhanced durability and corrosion resistance, particularly in marine environments, making the S35F20 mixture a promising choice for long-lasting concrete structures.

Funding

This research is financially supported by the Ministry of Transportation, Vietnam under project number DT203016.

Conflicts of interest

The authors declare no conflict of interest.

References

[1] Quan, H. V. "Ảnh hưởng của chất kết dính đến độ rỗng và hệ số suy giảm khuếch tán clorua của HPC" (The effect of the binder on porosity and chloride diffusion decay coefficient of HPC), Transport and Communications Science Journal, 71(9), pp. 1120–1129, 2020. (in Vietnamese) https://doi.org/10.47869/tcsj.71.9.10

[2] Uthaman, S., George, R. P., Vishwakarma, V., Harilal, M., Philip, J. "Enhanced seawater corrosion resistance of reinforcement in nanophase modified fly ash concrete", Construction and Building Materials, 221, pp. 232–243, 2019. https://doi.org/10.1016/j.conbuildmat.2019.06.070

[3] Zafar, I., Alqahtani, F. K. "Effectiveness of extended curing for fly ash concrete against corrosion propagation under severe chloride exposure", Structural Concrete, 22(5), pp. 2688–2703, 2021. https://doi.org/10.1002/suco.202000614

[4] Boğa, A. R., Topçu, İ. B. "Influence of fly ash on corrosion resistance and chloride ion permeability of concrete", Construction and Building Materials, 31, pp. 258–264, 2012. https://doi.org/10.1016/j.conbuildmat.2011.12.106

[5] Rooby, D. R., Kumar, T. N., Harilal, M., Sofia, S., George, R. P., Philip, J. "Enhanced corrosion protection of reinforcement steel with nanomaterial incorporated fly ash based cementitious coating", Construction and Building Materials, 275, 122130, 2021. https://doi.org/10.1016/j.conbuildmat.2020.122130

[6] Topçu, İ. B., Boğa, A. R. "Effect of ground granulate blast-furnace slag on corrosion performance of steel embedded in concrete", Materials & Design, 31(7), pp. 3358–3365, 2010. https://doi.org/10.1016/j.matdes.2010.01.057

[7] Thomas, M., Moffatt, E. "The Performance of Concrete in a Marine Environment", In: Proceedings of the sixth International Conference on Durability of Concrete Structures, West Yorkshire, United Kingdom, 2018, PL01. [online] Available at: https://docs.lib.purdue.edu/icdcs/2018/plenary/1/

[8] Hanh, D. K., Hien, D. T. T. "Tình trạng ăn mòn bê tông cốt thép và giải pháp chống ăn mòn cho công trình bê tông cốt thép trong môi trường biển Việt Nam" (Corrosion of reinforced concrete and the method to avoid corrosion for reinforced concrete structures in Vietnam's sea), Journal of Water Resources and Environmental Engineering, 11, pp. 44–49, 2011. [online] Available at: https://vjol.info.vn/index.php/DHTL/article/view/30212 (in Vietnamese)

[9] Tan, N. N., Dung T. A., The, N. C., Tuan, T. B., Anh, L. T. "Nghiên cứu thực nghiệm xác định ảnh hưởng của mức độ ăn mòn cốt thép đến ứng suất bám dính giữa bê tông và cốt thép" (Experimental study to determine the effect of reinforcement corrosion on adhesion stress between concrete and reinforcement), Journal of Science and Technology in Civil Engineering, 12, pp. 29–38, 2018. (in Vietnamese) https://doi.org/10.31814/stce.nuce2018-12(6)-04

[10] Huyen, B. T. T., Kien, T. T., Cuong, L. M., Minh, N. T., Phat, N. M. "Nghiên cứu đánh giá khả năng bảo vệ cốt thép của bê tông cường độ cao sử dụng hàm lượng tro bay lớn tiếp xúc với nước biển" (Research to evaluate the ability to protect steel reinforcement of high-strength concrete using high fly ash content in contact with sea water), Journal of Science and Technology in Civil Engineering, 15, pp. 94–110, 2021. (in Vietnamese) https://doi.org/10.31814/stce.huce(nuce)2021-15(6V)-09

[11] Huynh, T.-P., Ho, L. S., Ho, Q. V. "Experimental investigation on the performance of concrete incorporating fine dune sand and ground granulated blast-furnace slag", Construction and Building Materials, 347, 128512, 2022. https://doi.org/10.1016/j.conbuildmat.2022.128512

[12] Mehta, A., Siddique, R. "Sustainable geopolymer concrete using ground granulated blast furnace slag and rice husk ash: Strength and permeability properties", Journal of Cleaner Production, 205, pp. 49–57, 2018. https://doi.org/10.1016/j.jclepro.2018.08.313

[13] Ghosh, P, Tran, Q. "Influence of parameters on surface resistivity of concrete", Cement and Concrete Composites, 62, pp. 134–145, 2015. https://doi.org/10.1016/j.cemconcomp.2015.06.003

[14] Tran, Q., Ghosh, P. "Influence of pumice on mechanical properties and durability of high performance concrete", Construction and Building Materials, 249, 118741, 2020. https://doi.org/10.1016/j.conbuildmat.2020.118741

[15] Tran, Q., Ghosh, P. "Variation of electrical resistivity and charge passed in high-performance concrete", Materials, 15(9), 6694, 2022. https://doi.org/10.3390/ma15196694

[16] Yeau, K. Y., Kim, E. K. "An experimental study on corrosion resistance of concrete with ground granulate blast-furnace slag", Cement and Concrete Research, 35(7), pp. 1391–1399, 2005. https://doi.org/10.1016/j.cemconres.2004.11.010

[17] Cheng, A., Huang, R., Wu, J.-K., Chen, C.-H. "Influence of GGBS on durability and corrosion behavior of reinforced concrete", Materials Chemistry and Physics, 93(2–3), pp. 404–411, 2005. https://doi.org/10.1016/j.matchemphys.2005.03.043

[18] Zafar, I., Sugiyama, T. "Laboratory investigation to study the corrosion initiation of rebars in fly ash concrete", Magazine of Concrete Research, 66(20), pp. 1051–1064, 2014. https://doi.org/10.1680/macr.14.00069

[19] Montemor, M. F., Simões, A. M. P., Salta, M. M. "Effect of fly ash on concrete reinforcement corrosion studied by EIS", Cement and Concrete Composites, 22(3), pp. 175–185, 2000. https://doi.org/10.1016/S0958-9465(00)00003-2

[20] Hussain, R. R., Alhozaimy, A. M., Al-Negheimish, A. "Role of scoria natural pozzolan in the passive film development for steel rebars in chloride-contaminated concrete environment", Construction and Building Materials, 357, 129335, 2022. https://doi.org/10.1016/j.conbuildmat.2022.129335

[21] Sun, W., Zhang, Y., Liu, S., Zhang, Y. "The influence of mineral admixtures on resistance to corrosion of steel bars in green high-performance concrete", Cement and Concrete Research, 34(10), pp. 1781–1785, 2004. https://doi.org/10.1016/j.cemconres.2004.01.008

[22] Saraswathy, V., Song, H.-W. "Effectiveness of fly ash activation on the corrosion performance of steel embedded in concrete", Magazine of Concrete Research, 59(9), pp. 651–661, 2007. https://doi.org/10.1680/macr.2007.59.9.651

[23] Saraswathy, V., Muralidharan, S., Thangavel, K., Srinivasan, S. "Influence of activated fly ash on corrosion-resistance and strength of concrete", Cement and Concrete Composites, 25(7), pp. 673–680, 2003. https://doi.org/10.1016/S0958-9465(02)00068-9

[24] Ha, T.-H., Muralidharan, S., Bae, J.-H., Ha, Y.-C., Lee, H.-G., Park, K.-W., Kim, D.-K. "Accelerated short-term techniques to evaluate the corrosion performance of steel in fly ash blended concrete", Building and Environment, 42(1), pp. 78–85, 2007. https://doi.org/10.1016/j.buildenv.2005.08.019

[25] Ministry of Science and Technology "TCVN 2682:2009 Portland cements - Specifications", Vietnam, 2009. [online] Available at: https://thuvienphapluat.vn/TCVN/Xay-dung/TCVN-2682-2009-Xi-mang-pooc-lang-Yeu-cau-ky-thuat-905028.aspx (in Vietnamese)

[26] Ministry of Science and Technology "TCVN 11586:2016 Ground granulated blast-furnace slag for concrete and mortar", Vietnam, 2016. [online] Available at: https://thuvienphapluat.vn/TCVN/Xay-dung/TCVN-11586-2016-Xi-hat-lo-cao-nghien-min-dung-cho-be-tong-va-vua-917686.aspx (in Vietnamese)

[27] Ministry of Science and Technology "TCVN 10302:2014 Activity admixture - Fly ash for concrete, mortar and cement", Vietnam, 2014. [online] Available at: https://thuvienphapluat.vn/TCVN/Xay-dung/TCVN-10302-2014-Phu-gia-hoat-tinh-tro-bay-dung-cho-be-tong-vua-xay-xi-mang-911154.aspx (in Vietnamese)

[28] Ministry of Science and Technology "TCVN 7570:2006 Aggregates for concrete and mortar - Specifications", Vietnam, 2006. [online] Available at: https://thuvienphapluat.vn/phap-luat-doanh-nghiep/bai-viet/tieu-chuan-quoc-gia-tcvn-7570-2006-cot-lieu-cho-be-tong-va-vua-yeu-cau-ky-thuat-6298.html (in Vietnamese)

[29] Ministry of Science and Technology "TCVN 4506:2012 Water for concrete and mortar - Technical specification", Vietnam, 2012. [online] Available at: https://thuvienphapluat.vn/TCVN/Xay-dung/TCVN-4506-2012-Nuoc-tron-be-tong-va-vua-Yeu-cau-ky-thuat-907350.aspx (in Vietnamese)

[30] ACI Committee 363 "211.4R-08: Guide for selecting proportions for high-strength concrete using Portland cement and other cementitious materials", American Concrete Institute, Farmington Hills, MI, USA, 211.4R-08, 2008. [online] Available at: https://www.concrete.org/publications/internationalconcreteabstractsportal/m/details/id/56326

[31] Bahedh, M. A., Jaafar, M. S. "Ultra high-performance concrete utilizing fly ash as cement replacement under autoclaving technique", Case Studies in Construction Materials, 9, e00202, 2018. https://doi.org/10.1016/j.cscm.2018.e00202

[32] Ministry of Science and Technology "TCVN 3105:2022 Fresh and hardened concrete - Sampling, making and curing of test specimens", Vietnam, 2022. [online] Available at: https://thuvienphapluat.vn/phap-luat-doanh-nghiep/bai-viet/tieu-chuan-quoc-gia-tcvn-3105-2022-hon-hop-be-tong-va-be-tong-lay-mau-che-tao-va-bao-duong-mau-thu-4661.html (in Vietnamese)

[33] Ministry of Science and Technology "TCVN 3118:2022 Hardened concrete - Test method for compressive strength", Vietnam, 2022. [online] Available at: https://thuvienphapluat.vn/phap-luat-doanh-nghiep/bai-viet/tieu-chuan-quoc-gia-tcvn-3118-2022-be-tong-phuong-phap-xac-dinh-cuong-do-chiu-nen-6226.html (in Vietnamese)

[34] American Society for Testing and Materials "ASTM C496-96 Standard test method for splitting tensile strength of cylindrical concrete specimens", ASTM International, West Conshohocken, USA, 1996. https://doi.org/10.1520/C0496-96

[35] American Society for Testing and Materials "ASTM C642-21 Standard test method for density, absorption, and voids in hardened concrete", ASTM International, West Conshohocken, USA, 2021. https://doi.org/10.1520/C0642-21

[36] American Society for Testing and Materials "ASTM C1202-19 Standard test method for electrical indication of concrete's ability to resist chloride Ion penetration", ASTM International, West Conshohocken, USA, 2019. https://doi.org/10.1520/C1202-19

[37] American Associate of State Highway and Transportation Official "AASHTO TP95 Standard method of test for surface resistivity indication of concrete's ability to resist chloride ion penetration", AASHTO, Washington, D.C., USA, 2014. [online] Available at: https://global.ihs.com/doc_detail.cfm?document_name=AASHTO%20TP%2095&item_s_key=00577114

[38] Nordtest "Concrete, repairing materials and protective coating: Embedded steel method, chloride permeability (NT BUILD 356)", Nordtest, Espoo, Finland, Rep. NT BUILD 356, 1989. [online] Available at: https://www.nordtest.info/wp/1989/11/22/concrete-repairing-materials-and-protective-coating-embedded-steel-method-chloride-permeability-nt-build-356/

[39] Ministry of Science and Technology "TCVN 12041:2017 Concrete and reinforced concrete structures – General requirements for design durability and service life in corrosive environments", Vietnam, 2022. [online] Available at: https://thuvienphapluat.vn/TCVN/Xay-dung/TCVN-12041-2017-Ket-cau-be-tong-va-be-tong-cot-thep-Yeu-cau-chung-ve-thiet-ke-917346.aspx (in Vietnamese)

[40] Ehlen, M. A. "Life-365TM Service Life Prediction Model™ and Computer Program for Predicting the Service Life and Life-Cycle Cost of Reinforced Concrete Exposed to Chlorides", [pdf] ACI Committe 365, 2020. Available at: http://www.life-365.org/download/Life-365_v2.2.3_Users_Manual.pdf

[41] Tran, Q., Ghosh, P., Lehner, P., Konečný, P. "Determination of Time Dependent Diffusion Coefficient Aging Factor of HPC Mixtures", Key Engineering Materials, 832, pp. 11–20, 2020. https://doi.org/10.4028/www.scientific.net/KEM.832.11

[42] Konečný, P., Lehner, P., Ghosh, P., Tran, Q. "Variation of Diffusion Coefficient for Selected Binary and Ternary Concrete Mixtures Considering Concrete Aging Effect", Key Engineering Materials, 761, pp. 144–147, 2018. https://doi.org/10.4028/www.scientific.net/KEM.761.144

[43] Costa, A., Appleton, J. "Chloride penetration into concrete in marine environment-Part II: Prediction of long term chloride penetration", Materials and Structures, 32(5), pp. 354–359, 1999. https://doi.org/10.1007/BF02479627

[44] Swamy, R., Hamada, H., Laiw, J. C. "A Critical Evaluation of Chloride Penetration into Concrete in Marine Environment", In: Corrosion and Corrosion Protection Steel in Concrete: Proceedings of the International Conference on Corrosion and Corrosion Protection of Steel in Concrete, Sheffield, United Kingdom, 1994, pp. 404–419. ISBN 9781850757238 [online] Available at: https://xueshu.baidu.com/usercenter/paper/show?paperid=f739e819e5ce49a34da683432a654816

[45] Berke, N., Hicks, M. "Estimating the life cycle of reinforced concrete decks and marine piles using laboratory diffusion and corrosion data", ASTM International, West Conshohocken, USA, STP19764S, 1992. https://doi.org/10.1520/STP19764S

[46] Honglei, C., Zuquan, J., Tiejun, Z., Benzhen, W., Zhe, L., Jian, L. "Capillary suction induced water absorption and chloride transport in non-saturated concrete: The influence of humidity, mineral admixtures and sulfate ions", Construction and Building Materials, 236, 117581, 2020. https://doi.org/10.1016/j.conbuildmat.2019.117581

[47] Wang, J. L., Niu, K. M., Yang, Z. F., Zhou, M. K., Sun, L. Q., Ke, G. J. "Effects of fly ash and ground granulated blast-furnaces slag on properties of high-strength concrete", Key Engineering Materials, 405–406, pp. 219–225, 2009. https://doi.org/10.4028/www.scientific.net/KEM.405-406.219

[48] Wang, J., Basheer, P. A. M., Nanukuttan, S. V., Long, A. E., Bai, Y. "Influence of service loading and the resulting micro-cracks on chloride resistance of concrete", Construction and Building Materials, 108, pp. 56–66, 2016. https://doi.org/10.1016/j.conbuildmat.2016.01.005